Elastic constants and related properties of tetrahedrally bonded BN, AlN, GaN, and InN

Kwiseon Kim, Walter R. L. Lambrecht, and Benjamin Segall

Department of Physics, Case Western Reserve University, Cleveland, Ohio 44106-7079

The results of first-principles full-potential linear muffin-tin orbital calculations of the elastic constants and related structural and electronic properties of BN, AlN, GaN, and InN in both the zinc-blende and wurtzite structures are presented. The results include all of the equilibrium lattice constants, the bulk moduli, the TO-phonon frequencies at Γ, their mode Grüneisen parameters, the full set of cubic elastic constants, and deformation potentials. The elastic constants for the wurtzite crystals are first obtained from those calculated for zinc blende by Martin's transformation method. The components related to strains along the c axis (C_{13} and C_{33}) are found to be less accurate than the others. An elaboration of Martin's approach utilizing first-principles calculation for distortions which maintains hexagonal symmetry but allows for a nonideal c/a ratio is implemented. As a byproduct of the relaxation calculations of the wurtzite internal parameter u we also obtain the A_1 and an estimate of the E_1 TO-phonon frequencies in the hexagonal materials. Good agreement is obtained with recent experimental results for the elastic constants of wurtzite AlN and GaN and zinc-blende BN as well as for the other properties mentioned above for all materials. Our results provide predictions for the remaining crystal structure materials combinations for which no direct experimental data are presently available. From these results and experimental LO-TO splittings, we determine the bond-stretching and bond-bending parameters α and β of Keating's semiempirical valence-force-field model. We use this model to rationalize some of the observed trends in the behavior with the cation. The shift and splittings of the energy bands due to strains are used to obtain a complete set of deformation potentials for the zinc-blende crystals at symmetry points for several of the important eigenvalues. We also define deformation potentials for the valence-band maximum of the wurtzite structure and relate them to the corresponding [111] strain deformation and optical mode deformation potentials in zinc blende. [S0163-1829(96)00324-4]

I. INTRODUCTION

The group III nitrides are currently being actively investigated in view of the promising potentialities of AlN, GaN, and InN for short-wavelength electroluminescent devices and the extreme hardness and high thermal conductivity of c-BN. All these materials also have potential for high-temperature, high-power, and high-frequency electronics. These properties are closely related to their wide band gaps and strong (mixed ionic and covalent) bonding. An overview of the recent interest in wide-band-gap semiconductors and the particular role of the group III nitrides can be found in several recent conference proceedings[1–4] while general information on the properties of group III nitrides is available in a recent compilation.[5]

In order to model the behavior of the thin film heterostructures on which many electroluminescent devices [light-emitting diodes (LED) and laser diodes] are based, a knowledge of their elastic constants and strain deformation potentials is indispensable. For example, the elastic constants allow one to determine by continuum elasticity theory[6] the precise strain state of a pseudomorphic epitaxial thin film (which is under biaxial stress because it has to adapt to the substrate on which it is grown), or of a free standing superlattice of alternating thin layers of two of these binary materials. The pseudomorphic state is only expected to occur below the critical thickness, which is likely to be very small for any pair of these materials because of their sizable lattice mismatches, but may be relevant for interfaces between alloys among these materials with compositions close to each

other. One can use interpolated elastic constants for the alloys to deal with this situation. Above the critical thickness, misfit dislocations occur at the interface and relax the strain. Even in that case, the elastic constants may be needed to calculate the residual strain that may result from thermal expansion coefficient mismatch. In other words, films may be free of strain at the growth temperature but have a residual strain after cooling down. Once the strain state is determined, the deformation potentials determine the changes in the band structure resulting from the strain in the materials. Likewise, for the applications of c-BN in hard coatings and other applications related to its hardness, its elastic constants are obviously important.

Nevertheless, these properties are at present poorly known for all these materials. Although several total energy and band-structure calculations of the group III nitrides have recently been published (see, e.g., Ref. 7 for an overview), a systematic study of their elastic constants and behavior under hydrostatic and uniaxial stress has been lacking.

Until recently there were only a few fairly old experimental studies of the wurtzite nitrides (BN, GaN, and InN) (Ref. 8) which determined the elastic constants from rather indirect x-ray measurements on powders or crystals of rather poor quality. The values for cubic GaN and InN reported by Sherwin and Drummond[9] were obtained from these values by an appropriate rotation of the elasticity tensor for the hexagonal system. This procedure will be discussed below. Only recently have accurate values based on sound velocity or related measurements been reported for AlN,[10,11] GaN,[12] and c-BN.[13] Accurate measurements are still lacking for InN. In

good part this situation is due to the lack of good quality bulk single crystals of sufficient size. This situation may not be remedied very soon because most of the present research activity focuses on epitaxial films. Also, the nitrides are notoriously difficult to grow as single crystals from a melt because of the high partial pressure of N_2 required to prevent decomposition into N_2 and the group III metals.[14] This enhances the relevance of a theoretical determination of these important quantities.

Virtually no knowledge is available on the deformation potentials aside from a few calculated values for the change of band gap under hydrostatic strain. A critical review of previous band-structure calculations including values for the hydrostatic band-gap deformation potentials can be found in Ref. 7.

In this paper we present a systematic study of the elastic constants and related properties in both the zinc-blende and wurtzite polytypes. Results for zinc-blende GaN were reported earlier.[15] Although the natural polytype of AlN, GaN, and InN is wurtzite, the zinc-blende phase has been epitaxially stabilized for GaN and InN and has been observed for AlN in the form of precipitates resulting from ion implantation in fcc Al. BN in its tetrahedrally bonded form normally has the zinc-blende structure (usually called c-BN). The wurtzitic form appears to have been observed only in shock compression experiments. Besides these two structures, BN also has a layered hexagonal phase (called h-BN) which is similar to graphite. That form will not be considered here. (See Ref. 5, Chaps. 2 and 4 for further information and original references for each material.)

Our approach is to first calculate the elastic constants of the cubic phase (zinc blende). This is done by calculating the total energy as a function of strain for hydrostatic and traceless tetragonal and trigonal distortions. These calculations, respectively, provide $B=(C_{11}^c+2C_{12}^c)/3$, $C_s^c=(C_{11}^c-C_{12}^c)/2$, and C_{44}^c. To avoid confusion with the hexagonal tensor components to be discussed later, a superscript c for cubic and h for hexagonal is added. The total energies and the band structures are obtained from the density functional theory in the local density approximation[16] by means of the full-potential linear muffin-tin-orbital (FP-LMTO) method.[17,18] For the trigonal distortion, the internal parameter (the so-called Kleinman ζ parameter[19]) is relaxed. In the unstrained state, the related calculation of the energy as a function of the relative position of the two fcc sublattices of the zinc-blende structure provides information on the transverse-optical-phonon frequency at Γ (ω_{TO}^c). Repeating this calculation for a few volumes provides information on the pressure dependence of this important Raman observable phonon, which, for small volume changes, can be described by the usual mode Grüneisen parameter (γ_{TO}^c). The calculations provide values for these properties in addition to those for the elastic constants.

For the wurtzite elastic constants, we use a combination of first-principles calculations and the tensor transformation method of Martin.[20] As is well known, the two crystal structures are closely related with the (0001) plane of wurtzite being similar to the (111) plane of zinc blende and the $[10\bar{1}]$ direction in that plane in zinc blende being equivalent to the $[11\bar{2}0]$ direction in the wurtzite. As a consequence, a

simple rotation of the elastic constant tensor for the cubic phase to a new coordinate system with the z axis along [111] and the x axis along $[10\bar{1}]$ already provides a first approximation to the elastic constant tensor for the hexagonal material. The difference between the trigonal and the hexagonal systems is that in the hexagonal system $C_{14}^h=0$ while in the trigonal system it does not vanish. In addition, Martin took into account the fact that the tetrahedral building blocks in wurtzite are twinned with respect to those in the zinc-blende structure and hence they can undergo an internal distortion for certain strains. By minimizing the energy with respect to this internal strain, he obtained a correction term to the tensor components which is small for most components and exactly zero for C_{13}^h and C_{33}^h. The resultant transformation is summarized by

$$
\begin{pmatrix} C_{11}^h \\ C_{12}^h \\ C_{13}^h \\ C_{33}^h \\ C_{44}^h \\ C_{66}^h \end{pmatrix} = \frac{1}{6} \begin{pmatrix} 3 & 3 & 6 \\ 1 & 5 & -2 \\ 2 & 4 & -4 \\ 2 & 4 & 8 \\ 2 & -2 & 2 \\ 1 & -1 & 4 \end{pmatrix} \begin{pmatrix} C_{11}^c \\ C_{12}^c \\ C_{44}^c \end{pmatrix} - \begin{pmatrix} D/\bar{C}_{44}^h \\ -D/\bar{C}_{44}^h \\ 0 \\ 0 \\ D/\bar{C}_{66}^h \\ D/\bar{C}_{44}^h \end{pmatrix},
$$

where the $\bar{C}_{ij}^h$ are the values obtained without the second term (corresponding to rotation only), $D=\frac{2}{9}(C_{11}^c-C_{12}^c-C_{44}^c)^2$, and $\bar{C}_{66}^h=(C_{11}^h-C_{12}^h)/2$.

Our calculations show that several of the elastic constants of wurtzite obtained in this manner are in quite good agreement with experiment. However, there are two components, C_{33}^h and C_{13}^h, for which the discrepancies are appreciable. Both of these components are closely related to distortions along the c axis. Since the ideal c/a ratio is implied in Martin's approach, we surmised that deviations from it would play a significant role. We thus performed calculations of the elastic constants of the wurtzite structure involved in the distortion along the c axis which maintain the hexagonal symmetry, after first relaxing the structure with respect to $\eta \equiv c/a$ and the internal parameter u.

The traceless (fixed volume) c/a distortion provides the combination

$$C^h = C_{33}^h - 2C_{13}^h + (C_{11}^h + C_{12}^h)/2. \tag{1}$$

On the other hand, varying c with constant a yields C_{33}^h by itself. From these two calculations and the assumption that C_{11}^h and C_{12}^h are given correctly by the transformation, we obtain C_{13}^h. The explicit calculation of the wurtzite bulk modulus B with the structure relaxed as a function of c/a and u at each volume provides a further relation between the wurtzite elastic constants.

$$B^h = \frac{C_{33}^h(C_{11}^h+C_{12}^h)-2(C_{13}^h)^2}{C_{11}^h+C_{12}^h+2C_{33}^h-4C_{13}^h}, \tag{2}$$

which is used as an internal check of the calculation's accuracy.

We will show that the above procedure gives good agreement with the recently measured values for wurtzite AlN and GaN. Excellent agreement was also obtained for the full set

of cubic elastic constants of c-BN. For the remaining cases, wurtzite BN, zinc-blende GaN and AlN, and both structures of InN, our calculations provide predictions.

In the course of performing the relaxation calculations of the wurtzite with respect to the internal parameter u which determines the position of the anion relative to the cation sublattice, we obtain the TO-phonon frequency of symmetry A_1. The C^h elastic constant, given in Eq. (1), is obtained as a byproduct of the relaxation with respect to u and c/a. We find that u and c/a are strongly correlated. A relation is derived between the slope (ξ) of u as a function of c/a, the A_1 phonon frequency, and the elastic constants C^h and C_0^h defined in Eq. (1), respectively, in the presence and in the absence of internal relaxation. This generalizes a well-known relation for cubic materials between the C_{44}^c elastic constant, the TO-phonon frequency at Γ, and the Kleinman ζ parameter.

By using the approximate relation between TO phonons in the cubic structure (of symmetry T_2) and hexagonal structure (of symmetry A_1 and E_1),

$$\omega_{T_2}^2 = (\omega_{A_1}^2 + 2\omega_{E_1}^2)/3, \tag{3}$$

and our calculated values for the cubic T_2 and hexagonal A_1 modes, we also obtain approximate values for the E_1 phonon.

By analyzing the band structures for the materials in equilibrium and subject to the small strain distortions used in the calculation of the elastic constants, we obtain the so-called deformation potentials. These describe the shifts and splittings of the band-structure eigenvalues to linear order in the strain. A systematic group-theoretical analysis was provided for cubic materials by Kane.[21] As for any tensor, an arbitrary strain can be reduced into irreducible components. Using these and the irreducible representation of the specific eigenstate under study, one obtains the complete set of deformation potentials for that state. From those, the behavior of the state under any arbitrary strain state can be deduced. This information is perhaps most important for the band edges since these determine the band gaps and the band offsets at heterojunctions. However, it is also of some relevance for other eigenstates such as those involved in important critical point optical transitions. In fact, these deformation potentials describe essentially the elasto-optic behavior of such transitions. The strain deformation potentials described here are also the long-wavelength limit of the electron-phonon coupling parameters for acoustic phonons and as such are relevant to transport theory for the states near the band edges.

We emphasize that for all traceless strains, i.e., uniaxial and volume conserving strains, the deformation potentials of individual eigenvalues can be directly obtained from bulk calculations. However, for the hydrostatic strain, only relative deformation potentials, i.e., differences between those for different eigenstates, are meaningful. Because the electrostatic reference level of an infinite periodic solid is ill defined, the absolute deformation potentials under hydrostatic strain only obtain meaning as the long-wavelength limit of acoustic phonons. They are thus direction dependent. And, an interface calculation is required to take into account the effects of charge transfer between compressed and expanded regions of the crystal. A detailed study of this is

postponed to a future work. Here, we only present the values obtained within a simple orientation independent treatment of the band lineup problem between the compressed and expanded regions of the crystal provided by the so-called dielectric midpoint energy model (DME).[22]

In order to allow for an easy comparison of the various properties among the different materials in the class of the group III nitrides, the results are organized by materials property. A brief description of some of the relevant computational details is given in Sec. II followed by a discussion of the relationship between the A_1 TO-phonon and hexagonal elastic constants for wurtzite in Sec. III. We present our results for the lattice constants in Sec. IV A, the bulk moduli in Sec. IV B, the TO-phonon frequencies and their pressure dependencies in Sec. IV C, the internal strain parameters (ζ and ξ) in Sec. IV D, and the elastic constants in Sec. IV E. Values are presented both for the zinc-blende and wurtzite structures. We then discuss the trend of these elastic properties by first extracting the bond-stretching and bond-bending parameters of the well-known Keating model in Secs. IV F and IV G. The essential ingredients parametrizing the Keating model are indeed the cubic elastic constants and the TO-phonon–LO-phonon splittings which provide information on the long-range Coulomb effects. The splittings, which as yet have not been calculated, are taken from experiment. The Keating model in fact presumes certain relations between the cubic elastic constants. We discuss the degree of validity of these for the present materials. We also discuss the application of the Keating model to the wurtzite form. Although it is obviously not capable of reproducing the nonideal c/a ratios, it does a fair job at reproducing the relation between the c/a and internal parameter u of the wurtzite. After this discussion, we turn to the electronic properties. We present a rather complete set of deformation potentials for several of the important band states in zinc blende in Sec. V B. For the convenience of the reader, we provide explicit definitions of all the deformation potentials in question and their relation to some other frequently used notations in Sec. V A. We also define deformation potentials for the valence-band maximum of the wurtzite structure under c/a distortion and the transverse-optical A_1 mode and relate them to the [111] strain and optical mode deformation potentials in zinc blende.

II. COMPUTATIONAL METHOD

The calculations were performed *ab initio* within the local density approximation (LDA) to the density functional theory[16] using the Hedin-Lundqvist parametrization of exchange correlation[23] and the full-potential linear muffin-tin-orbital method.[17,18]

A multiple-κ muffin-tin-orbital (MTO) basis set is used, where κ^2 is the kinetic energy of the MTO envelope function. A MTO consists of a linear combination of the radial Schrödinger equation solution and its energy derivative matched continuously and differentially onto the envelope function at the muffin-tin-sphere radii. Three augmented Hankel functions with decay energies κ^2 of -0.01, -1.0, and -2.3 Ry were used. The charge density and potential in the interstitial region are expressed as expansions in a separate set of Hankel functions centered on all spheres.[18] For

TABLE I. Basis vectors and inequivalent atomic and empty sphere positions in zinc blende and wurtzite, in units of the cubic lattice constant for zinc blende, a_c, and the hexagonal in-plane lattice constant, a_h. In wurtzite a second set of atoms is obtained by applying a sixfold screw rotation.

	Zinc blende	Wurtzite
a_1	0, 1/2, 1/2	1, 0, 0
a_2	1/2, 0, 1/2	1/2, $\sqrt{3}/2$, 0
a_3	1/2, 1/2, 0	0, 0, η
cation	0, 0, 0	0, 0, 0
anion	1/4, 1/4, 1/4	0, 0, $u\eta$
e_1	1/2, 1/2, 1/2	0, 0, $(u+1)\eta/2$
e_2	3/4, 3/4, 3/4	0, $1/\sqrt{3}$, $u\eta/2$

these, two decay energies ($\kappa^2 = -1.0$ and -3.0 Ry) are chosen and an angular momentum cutoff of $l=4(5)$ was found to be adequate for zinc blende (wurtzite).

In order to keep the interstitial volume small, empty spheres are added to these open structures. The positions of the empty spheres for zinc blende and wurtzite are given in Table I, which contains the structural information. The positions of the atomic and empty spheres in wurtzite are shown in Fig. 1. The radii of the muffin-tin spheres were usually chosen so that they stay fixed and nonoverlapping under the imposed distortions. (Radii were chosen as 95–97 % of touching.) Under hydrostatic volume changes they were scaled with the volume. The reason for keeping constant sphere radii during distortions is that there are small numerical errors related to the fitting of the quantities in the interstitial region. These errors scale with the interstitial volume. By keeping the latter constant, those errors are expected to cancel in the energy differences related to the distortion. We allowed one exception to this rule. For the wurtzite c/a relaxation, we found that keeping the sphere radius of the small empty sphere e_1 fixed was not always satisfactory. An improvement in the results for c/a resulted from allowing
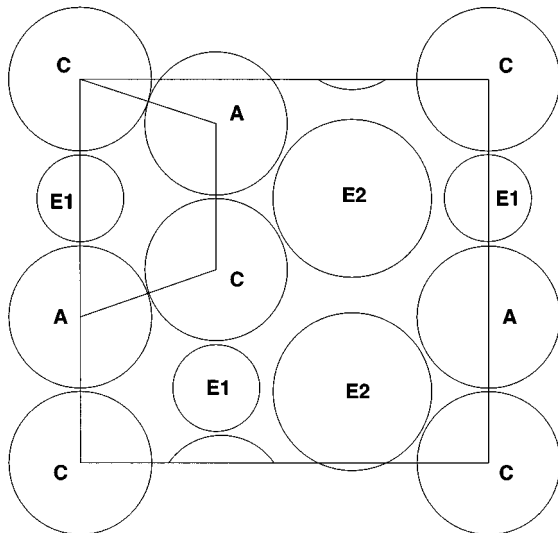
FIG. 1. Atomic and empty sphere positions in wurtzite: projection on a $(\bar{1}100)$ plane.

that sphere to change size so as to remain nearly touching. This was found to be the case primarily for InN, where the relaxation will be shown to be mostly a bond angle variation. This leads to a large *local* variation in the interstitial volume near that sphere. On the other hand, the energy is not very sensitive to the choice of the radius of the sphere in the open channel (e_2). We conclude that it is more important to keep the volume of the interstitial region constant in the regions of high charge density rather than overall interstitial volume. For GaN the results were also slightly improved by adopting a variable size e_1 sphere, while for AlN and BN there was no change.

The basis set used for all the zinc-blende calculations has MTO's centered only on the real atoms (not on the empty spheres), implying a total of 27 orbitals per atom for the ddd basis set used. The notation ddd means the inclusion of angular momenta up to $l=2$ for each κ. This basis set was previously found to be accurate for most zinc-blende crystals. For wurtzite, because of the demanding accuracy for the c/a and u relaxation, a separate convergence study was undertaken. The basis set used for the final calculations is described by fdp on the atoms and s on the large empty sphere e_2. Even if no basis functions were centered on all empty spheres, the MTO orbitals were of course augmented in all empty spheres, i.e., the Hankel function tail of a function centered on one site is expanded in spherical harmonics around other sites and replaced by an appropriate linear combination of the solutions of the radial Schrödinger equation and their energy derivatives. An angular momentum cutoff of $l=4$ in zinc blende and $l=5$ in wurtzite, equal to the cutoff for the interstitial expansion set, was used for these expansions.

Due to the dispersion of Ga $3d$ states and their hybridization with N $2s$ it is necessary to treat the former as bands.[24–26] Similarly, the In $4d$ are treated as bands for InN. The results were obtained nonrelativistically except for InN where the scalar relativistic version of the FP-LMTO method was used. For the properties considered, the relativistic corrections for BN, AlN, and GaN are negligible. The Brillouin zone summations were performed with an adequately converged set of ten special points[27] for zinc blende and 36 points for wurtzite. For the calculations of zinc blende under uniaxial distortions, a correspondingly larger set of inequivalent k points was used as required by the lower symmetry.

To calculate the cubic elastic constants, the total energies under hydrostatic, tetragonal, and trigonal strains were calculated using strains up to 6%. For each strain the total energy differences between the strained and the unstrained states were fitted to a parabola. In effect, this means that the elastic constants were obtained from numerical second derivatives of the total energy differences. For the u relaxation, we used the Harris approach[28,29] to calculate forces. In this approach the self-consistent charge density at the structure from which the force is to be calculated is decomposed into a superposition of overlapping atom-centered (but not necessarily spherically symmetric) charge densities. Those are then displaced rigidly and appropriately by a small amount δx for the structural distortion under consideration. The total energy at two displaced configurations ($\pm \delta x$) is then calculated non-self-consistently via the Harris functional, and the force (or rather gradient with respect to parameter x) is ob-

tained numerically as $\partial E/\partial x = [E(x_0 + \delta x) - E(x_0 - \delta x)]/2\delta x$. Once we are within the harmonic region, the force at one point and the knowledge of the equilibrium point immediately give the force constant or the second derivative. The fully self-consistent numerical and Harris gradient approaches were found to be in good agreement. In principle, the latter approach could be used for the c/a relaxation as well. However, because of the difficulties encountered for it, we preferred to use the fully self-consistently calculated total energies.

III. RELATIONS BETWEEN ELASTIC CONSTANTS AND PHONONS FOR WURTZITE

The wurtzite structure is fully determined by two lattice constants a and c, or, equivalently, the volume of the unit cell $V = \sqrt{3}/2 \, a^2 c$ and $\eta = c/a$ ratio, and one internal parameter u defined such that the cation-anion nearest neighbor bond length along the c axis is given by $d = uc$. Thus the total energy must be minimized as a function of three parameters. For a given cell volume V, consider the expansion of the energy $E(\eta, u)$ in a Taylor series around the equilibrium values η_0 and u_0,

$$
\begin{aligned}
E(\eta, u) = &\, E(\eta_0, u_0) + \frac{1}{2}\delta u^2 \frac{\partial^2 E}{\partial u^2} \\
&+ \delta u\, \delta \eta \frac{\partial^2 E}{\partial u\, \partial \eta} + \frac{1}{2}\delta\eta^2 \frac{\partial^2 E}{\partial\eta^2} \\
= &\, E_0 + \frac{1}{2}\delta u^2 c^2 \Phi + \delta u\, \delta\eta c\Omega D + \frac{1}{2}\delta\eta^2 \Omega C_{\eta,0},
\end{aligned}
$$
(4)

where the second form introduces a force constant matrix Φ, an internal strain matrix D, and an "unrelaxed" elastic constant $C_{\eta,0}$. The volume of the unit cell Ω and c is introduced so as to give Φ and $C_{\eta,0}$ the correct physical dimensions. Indeed, the second derivative with respect to the internal parameter u basically defines an "atomic force," while the second derivative with respect to the external cell parameter η defines an elastic constant in the absence of internal relaxation. The off-diagonal partial second derivative determines the coupling between the strain and the internal parameter and is thus related to internal strain. We can also rewrite it as $D = \Phi \xi c/\Omega$, introducing a new parameter ξ, the physical meaning of which will become clear in a moment.

The first derivatives of Eq. (4) with respect to cu and η define, respectively, a "force,"

$$
-F = c\,\delta u\,\Phi + \delta\eta\,\Omega D, \tag{5}
$$

and a "stress,"

$$
\sigma = \delta\eta C_{\eta,0} + c\,\delta u D. \tag{6}
$$

Minimizing the energy with respect to u for each value of η requires $F = 0$, or

$$
\delta u_{\min} = -(\Omega D/c\Phi)\delta\eta = -\xi\delta\eta, \tag{7}
$$

which makes clear that ξ is the slope of u_{min} as a function of η. Substituting Eq. (7) in Eq. (6), we obtain

$$
\sigma = \delta\eta(C_{\eta,0} - \Omega^{-1}\Phi c^2 \xi^2) = \delta\eta C_\eta, \tag{8}
$$

defining the true elastic constant C_η, including the effects of the internal relaxation. Noting that the force constant Φ determines the A_1 transverse-optical-phonon frequency through $\Phi = \mu(\omega_{TO}^{A1})^2$, with μ the reduced mass, we obtain

$$
C_\eta = C_{\eta,0} - \Omega^{-1}\mu(\omega_{TO}^{A1}\xi c)^2. \tag{9}
$$

This equation is the equivalent for the wurtzite of the well-known equation for zinc blende relating the C_{44}^c shear elastic constant for trigonal distortions to its unrelaxed value $C_{44,0}^c$, the transverse-optical-phonon frequency ω_{TO}^c, and the Kleinman ζ parameter,

$$
C_{44}^c = C_{44,0}^c - \Omega^{-1}\mu[\omega_{TO}^c\zeta(a/4)]^2. \tag{10}
$$

Equation (9) shows that ξ plays the same role for wurtzite as the Kleinman ζ parameter does for zinc blende.

To conclude this section, we note that for a traceless uniaxial distortion along the hexagonal c axis (i.e., a change of η for fixed volume), the strain tensor using the usual matrix notation for elasticity theory[30] is specified by

$$
\epsilon_1 = \epsilon_2 = -\epsilon/2,
$$

$$
\epsilon_3 = \epsilon,
$$

$$
\epsilon_4 = \epsilon_5 = \epsilon_6 = 0. \tag{11}
$$

This leads to the stress tensor with components,

$$
\sigma_1 = \sigma_2 = [C_{13}^h - (C_{11}^h + C_{12}^h)/2]\epsilon,
$$

$$
\sigma_3 = [C_{33}^h - C_{13}^h]\epsilon,
$$

$$
\sigma_4 = \sigma_5 = \sigma_6 = 0. \tag{12}
$$

Since, furthermore, we have $\eta' = (1+\epsilon)c/(1-\epsilon/2)a \approx (1+\frac{3}{2}\epsilon)\eta$, we obtain $\delta\eta/\eta = \frac{3}{2}\epsilon$, or

$$
\begin{aligned}
C^h &= \Omega^{-1}(\partial^2 E/\partial\epsilon^2) \\
&= C_{33}^h - 2C_{13}^h + (C_{11}^h + C_{12}^h)/2 \\
&= \frac{9}{4}\eta^2 \Omega^{-1}(\partial^2 E/\partial\eta^2)_{u_{\min}} \\
&= \frac{9}{4}\eta^2 C_\eta,
\end{aligned}
\tag{13}
$$

which provides a derivation of Eq. (1) and establishes its relation to the second derivative of E with respect to η.

Similarly, if we fix a and vary $c = (1+\epsilon)\eta_0 a$, the strain tensor is $(0,0,\epsilon,0,0,0)$, the stress tensor is $(C_{13}^h\epsilon, C_{13}^h\epsilon, C_{33}^h\epsilon, 0,0,0)$, and the elastic energy becomes $\frac{1}{2}\Omega C_{33}^h\epsilon^2$, so the curvature of E as function of c for fixed a yields directly C_{33}^h.

As an example, we show in Fig. 2 the total energy and $u_{\min}$ as a function of η for InN at the experimental equilibrium value V_0, from which $C^h(V_0)$ and $\xi(V_0)$ are derived. We find that the variation of ξ with volume can be ignored.

wurtzite InN

4d as band, In +N fdp Es, V=V₀
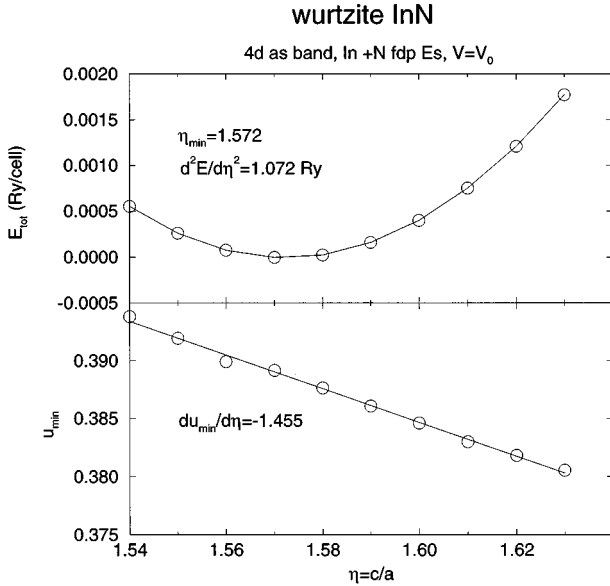
FIG. 2. Total energy (with respect to minimum) and $u_{\min}$ in wurtzite InN as a function of c/a at the experimental equilibrium volume.

IV. TOTAL ENERGY RELATED RESULTS

A. Lattice constants

Table II shows our calculated equilibrium lattice constants and compares them with experimental[5,31,32] and other computational results.[15,33–53] As usual, the LDA calculations slightly underestimate the lattice constants. The cubic and hexagonal lattice constants a_c and a_h are underestimated by about 1%. The c lattice constants are underestimated by 2–3% and hence the volumes by 3–5%, the c/a by 0.1–3%. The worst case for c/a occurs for InN. For that compound we noted above that the c/a relaxation is quite demanding because of the very small energy differences involved (because of the lower elastic constants, see below) and because of the predominance of bond-angle variation. Also, there is a considerable spread in experimental values.

Because there are a large number of computational results for the zinc-blende lattice constants, we indicate only the range of values that have been reported in Table II. For wurtzite, only a few calculations include a complete structure determination. We thus compare our results with two well-converged pseudopotential calculations, by Wright and Nelson[47] and by Yeh et al.,[46] the first one including the d states of Ga and In as bands, the second one treating them as core states. We note that the latter slightly overestimates the lattice constants in contrast to ours which obtain the more usual underestimate for the LDA. Our calculated wurtzite lattice constants for AlN is nearly identical to those obtained earlier by Christensen and Gorczyca[45] using the FP-LMTO method.

B. Bulk moduli

The bulk moduli are listed in Table III. Unfortunately, the ranges of values obtained in other calculations for the zinc-blende crystals and from experiments are quite large. Our values are in agreement with well-converged pseudopotential

calculations[47] to within a few percent. The deviations from the experimental values are as large as 15% but the various experiments differ among themselves by at least that much. The LDA generally overestimates bulk moduli. That this is not obvious here suggests that the experimental values should be considered to be somewhat uncertain. This is not surprising given that large single crystals are presently unavailable for these materials.

The differences between zinc-blende and wurtzite bulk moduli are smaller than the estimated error due to LDA and uncertainties associated with the computational differences between the two crystal structures (e.g., a different interstitial volume) and thus not considered to be significant. We emphasize that the $E(V)$ used here for wurtzite were fully relaxed values with respect to both c/a and u.

The present bulk moduli were obtained by fitting $E(V)$ to the equation of state curve of Rose et al.[62] This fit also provides the pressure derivative B'. However, the fitting is not very sensitive to B' over the range of volumes considered. The resulting error bar for B' is estimated to be about 0.5. Within this error bar there are no systematic changes with crystal structure nor with cation and a value of $B' \approx 4 \pm 0.5$ is deduced for all nitrides. This is in agreement with experiment for c-BN and for GaN, while somewhat larger values have appeared in the literature for AlN and InN. Since fitting of an equation of state to experimental $p(V)$ relations may introduce a correlated error in both B and B' values and a fairly large range of pressures is needed to determine B$'$ confidently, these values of B' should be considered somewhat uncertain.

As for the trend with materials, we may note that GaN and AlN have very similar bulk moduli while that of c-BN is substantially higher and that of InN is substantially lower.

C. Phonons

The transverse-optical-phonon frequencies at Γ are given in Table IV for the two polytypes. For wurtzite, we only calculated the A_1 phonon directly, the E_1 phonon being determined from Eq. (3). Our calculated values appear to overestimate the experimental values by about 1–5%. For zinc-blende GaN our value is slightly larger than that from the FP-LMTO calculation by Gorczyca et al.[63] and slightly smaller than that from the FP-LMTO calculation by Fiorentini, Methfessel, and Scheffler.[26] In the course of understanding the cause of the differences, we found that for relative displacements of 4% or larger anharmonic effects tend to increase the phonon frequency. Also, values obtained using the forces or the energies are found to differ from each other by about 20 cm^{-1}. We thus consider this number to be a conservative estimate of the numerical error bar on the results. With this in mind, the agreement of our calculation both with experiment and with the other calculations is seen to be quite good. In our calculations, we consider both stretched and compressed bonds. Using only stretched bonds would lead to lower values of the force constants and hence lower phonon frequencies. Our basis set is also slightly different from that used in Ref. 63.

Only one value is given for the mode Grüneisen parameter for each material, because we find the differences between the values for the various TO modes discussed here to be insignificant.

TABLE II. Lattice constants of zinc blende and wurtzite III nitrides (in Å).

		BN	AlN	GaN	InN
		Zinc blende			
Present		3.59	4.32	4.46	4.92
Other calculations		3.56–3.77[a]	4.33–4.42[b]	4.30–4.50[c]	4.93–4.98[d]
Experiment[e]		3.615	4.37	4.50[f]	4.98[g]
		Wurtzite			
Present	a	2.54	3.06	3.17	3.53
	c	4.17	4.91	5.13	5.54
	c/a	1.64	1.60	1.62	1.57
	u	0.375	0.383	0.379	0.388
Other calculations[h]	a		3.084	3.162	3.501
	c		4.948	5.142	5.669
	c/a		1.604	1.626	1.619
	u		0.3814	0.3770	0.3784
Other calculations[i]	a		3.099	3.095	3.536
	c		4.997	5.000	5.709
	c/a		1.612	1.633	1.615
	u		0.381	0.378	0.380
Experiment[j]	a		3.11	3.189	3.54–3.60
	c		4.98	5.185	5.69–5.76
	c/a		1.60	1.626	1.59–1.62

[a]References 33–43.
[b]References 43–48.
[c]References 15, 43, and 46–52.
[d]References 43, 46, 47, and 53.
[e]From Ref. 5, Chaps. 1, 4. Because of the unavailability of data for zinc-blende AlN, the tabulated value
 corresponds to the volume per atom in the wurtzite form.
[f]Lei *et al.* (Ref. 31).
[g]Strite *et al.* (Ref. 32).
[h]Pseudopotential with Ga $3d$ and In $4d$ by Wright and Nelson (Ref. 47).
[i]Pseudopotential without Ga $3d$ and In $4d$ by Yeh et al. (Ref. 46).
[j]From Ref. 5, Chaps. 1, 4.

D. Internal strain parameters

The well-known Kleinman ζ parameter for zinc blende and the ξ parameter for wurtzite introduced in Sec. III describe the relative positions of the cation and anion sublattices under volume conserving strain distortions in which the positions are not fixed by symmetry. These are trigonal distortions along [111] for zinc blende and hexagonal distortions for wurtzite. The calculated values for these parameters are given in Table V.

We recall that a low value of ζ or $|\xi|$ implies that there is a large resistance against bond-angle distortions while the reverse is true for a high value. The values for AlN and GaN, which are almost the same, are much larger than those for BN and smaller than those for InN. The importance of bond-angle forces in BN is similar to that in diamond.

E. Elastic constants

The results for the elastic constants of the nitrides in the zinc-blende structure are given in Table VI. Experimental data are only available for c-BN.[13] The agreement with experiment and with the only other first-principles calculation[42] is very good.

Our results for the elastic constants of the nitrides in the wurtzite structure are given in Table VII. Good agreement is obtained with the recent experimental data for AlN and GaN, the only two materials for which direct experimental data are available up to now.

It should be noted that other C_{ij} data for wurtzite BN, GaN, and InN were reported earlier.[8] These were obtained from analyses of temperature-dependent broadening of x-ray diffraction spectra from powders.[8] These values, obtained rather indirectly[70] differ markedly from those obtained from

TABLE III. Bulk moduli for zinc blende and wurtzite III nitrides.

		BN	AlN	GaN	InN
			Zinc blende		
Present	B	400	203	201	139
	B'	4.1	3.2	3.9	4.4
Other calculations	B	353–412[a]	195–228[b]	173–200[c]	137–161[d]
	B'	3.1–3.6[a]	3.9,4.0[e]	2.66–4.6[c]	3.9–4.3[d]
Experiment	B	369–382[f]			
	B'	4.0–4.5[f]			
			Wurtzite		
Present	B	397	202	207	146
	B'	3.7	3.8	4.5	3.4
Other calculations[g]	B		205	202	139
	B'				
Experiment	B		185–212[h]	188–245[i]	125[j]
	B'		5.7–6.3[h]	3.2–4.3[i]	12.7[j]

[a]From Refs. 33–43.
[b]From Refs. 43–45, 47, 48, and 54.
[c]From Refs. 15, 43, 47–50, and 52.
[d]From Refs. 43, 47, and 53.
[e]From Refs. 43 and 44.

[f]From Refs. 13, 38, 55, and 56.
[g]Wright and Nelson (Ref. 47).
[h]From Refs. 57–59.
[i]From Refs. 57, 60, and 61.
[j]Ueno *et al.* (Ref. 57).

the Brillouin scattering measurements and from the calculations. This is evident from Fig. 3 which compares all experimental C_{ij} with the corresponding calculated values. The figure also displays the overall agreement between the calculations and the velocity of sound based measurements. Because of the apparent imprecision of the earlier data,[8] it is excluded from the tables even though it contains the only data for InN.[70]

Figure 4 and the numbers in parentheses and square brackets in Table VII provide some detail on how the results for the elastic constants for wurtzite crystals depend on the computational model. The numbers in parentheses in Table VII for C_{11}^h, C_{12}^h, and C_{44}^h are the results obtained by simply rotating the cubic tensor to the coordinate system appropriate for the hexagonal crystals without applying the internal strain correction. We see that the internal strain term provides a sizable correction for the nitrides. The numbers in square brackets for C_{13}^h and C_{33}^h are the results obtained from the tensor rotation method without c/a and u relaxation. These are unaffected by the internal strain correction. However, it is evident that the actual (measured) values are strongly affected by the relaxation. Figure 4 shows that aside from C_{13} and C_{33}, the C_{ij} obtained by Martin's transformation method are in good accord with the experimental values. It also shows that most of the discrepancies between theory and experiment for C_{13} and C_{33} are removed by the structure relaxation.

At the bottom of Table VI we show the values of C_{44}^{c0}, the constant without the internal strain contribution. Similarly, in the bottom rows of Table VII, we give the values of the wurtzite elastic constants C^h and C^{h0} defined by Eq. (1) with and without the internal strain relaxation. The comparisons show that the coupling of these strain distortions to the optic phonon are quite important for all nitrides except for BN, where the bond-angle forces are large, or, alternatively, the values of ζ and $|\xi|$ are extremely low.

Finally, we show the bulk moduli as obtained from the C_{ij}. These values are in good agreement with those found from the direct calculations and presented in Sec. IV B.

F. Keating model parameters

The Keating model[71] is a frequently used semiempirical potential for tetrahedrally bonded semiconductors because of its simplicity. It is thus of interest to obtain its force constant parameters for the nitrides and to investigate the model's applicability to these materials. It was generalized for partially ionic zinc-blende crystals by Martin.[72] The elastic energy in the model is described in terms of bond-stretching and bond-bending force constant parameters, α and β, by

$$E_{el} = \frac{1}{2}\alpha\left(\frac{3}{4r^2}\right)\sum_{i=1}^{4}[\Delta(\mathbf{r}_i\cdot\mathbf{r}_i)]^2$$
$$+\frac{1}{2}\beta\left(\frac{3}{4r^2}\right)\sum_{i\neq j}[\Delta(\mathbf{r}_i\cdot\mathbf{r}_j)]^2, \quad (14)$$

where the first sum is over all bonds, the second is over all bond pairs centered on a given atom, $\mathbf{r}_i$ is the vector linking an atom to one of its four neighbors, and r is the equilibrium bond length. The parameters are determined by fitting the elastic constants and some phonon data as described below. The long-range Coulomb force, which produces the LO-phonon–TO-phonon splitting, is characterized by the effective charge parameter Z^* (or, equivalently S) through

$$S = Z^{*2}/\epsilon = (\Omega/4\pi e^2)\mu(\omega_l^2 - \omega_t^2). \quad (15)$$

Martin derived the following relations between the elastic constants and the Keating parameters:

$$C_{11} + 2C_{12} = (\sqrt{3}/4r)(3\alpha + \beta) - 0.355SC_0, \quad (16a)$$

TABLE IV. Transverse-optical-phonon frequencies at Γ for the group III nitrides (in cm^{-1} with our values rounded to the nearest 10 cm^{-1} because of the estimated error bar). To the precision of the calculations, the mode Grüneisen parameter γ is identical for the zinc-blende and wurtzite forms. It is thus only tabulated for the zinc-blende structures.

Symmetry		BN	AlN	GaN	InN
		Zinc blende			
T_2	present	1070	680	580	540
	other calculations	1000[a],1070[b]	648[c],652[d]	558[c], 551[d], 600[e]	
	experiment	1055[f], 1056[g,h]		556[i]	
		Wurtzite			
A_1	present	1040	610	570	450
	other calculations		601[c],629[d], 668[j]	534[c], 537[d]	
	experiment	1090[h]	607[k],614[h],659[f],660[l]	532[h]	400[m]
E_1	present	1080	710	585	580
	other calculations		650[c], 649[d], 734[j]	556[c],555[d]	
	experiment	1120[h]	673[h],672[f,l]	560[h]	490[m]
γ	present	1.2	1.5	1.8	1.5
	other calculations		1.42–1.50[d]	1.48–1.52[d]	
	experiment	1.5 [f,g]	1.58[k], 1.6[f]	1.53[n]	

[a]Pseudopotential LDA, Lam, Wentzcovitch, and Cohen (Ref. 37).
[b]Pseudopotential LDA, Rodriguez-Hernández, González-Diaz, and Muñoz (Ref. 42).
[c]Pseudopotential LDA, Miwa and Fukumoto (Ref. 48).
[d]FP-LMTO LDA, Gorczyca *et al.* (Ref. 63).
[e]FP-LMTO LDA, Fiorentini, Methfessel, and Scheffler (Ref. 26).
[f]Raman data, Sanjurjo *et al.* (Ref. 64).
[g]Raman data, Alvarenga, Grimsditch, and Polian (Ref. 56).
[h]From Ref. 5, Chap. 8.
[i]Raman data, Murugkar *et al.* (Ref. 65).
[j]Hartree-Fock, Ruiz, Alvarez, and Alemany (Ref. 54).
[k]Raman data for A_1 mode, Perlin, Polian, and Suski (Ref. 66).
[l]Raman data, Hayashi *et al.* (Ref. 67).
[m]Raman data, Inushima *et al.* (Ref. 68).
[n]Raman data for A_1 mode, Perlin *et al.* (Ref. 61).

$$C_{11}-C_{12}=(\sqrt{3}/r)\beta+0.053SC_0, \quad (16b)$$

$$C_{44}=(\sqrt{3}/4r)(\alpha+\beta)-0.136SC_0-C\zeta^2, \quad (16c)$$

where

$$C=(\sqrt{3}/4r)(\alpha+\beta)-0.266SC_0, \quad (17a)$$

$$\zeta=C^{-1}[(\sqrt{3}/4r)(\alpha-\beta)-0.294SC_0], \quad (17b)$$

$$C_0=e^2/r^4. \quad (17c)$$

Here, α and β are obtained from Eqs. (16a) and (16b) using our calculated C_{11} and C_{12} and S from Eq. (15) and the measured LO-phonon–TO-phonon splittings.[5] Equations

TABLE V. Internal strain parameters ζ and ξ for zinc blende and wurtzite, respectively.

	BN	AlN	GaN	InN
ζ	0.1	0.6	0.5	0.7
$-\xi$	0.00	0.12	0.11	0.14

(16c) and (17b) then give Keating model predictions for C_{44} and ζ. These are compared with the directly calculated values to gauge the validity of the Keating model for the nitrides. The relevant data, resulting parameters, and consistency checks are given in Table VIII. We note that the quality of the Keating model predictions for C_{44} deteriorates as we go down the series. However, the model gives a fair reproduction of the trend in ζ values. In particular, a low value of ζ for BN is found. An important parameter for the Keating model is β/α, which indicates the relative importance of bond-bending to bond-stretching forces. From the discussions in Sec. IV D, we see that the relatively large β/α for BN is consistent with its low value of ζ.

Although the Keating model is unable to predict the non-ideal c/a and u values for wurtzite, it can be used to find u_{min} as a function of c/a for a given ratio β/α. From that the model prediction for the ξ parameter can be found by Eq. (7). Figure 5 shows how the u_{min} varies with c/a for β/α which correspond to those obtained for BN, AlN, GaN, and InN as well as the pure bond-stretching limit $\beta=0$ and the (unrealistic) pure bond-bending limit $\alpha=0$. The values obtained for ξ are 0.06 for BN, 0.11 for AlN and GaN, 0.12 for InN, and 0.15 for $\beta=0$. These values are in fair agreement

TABLE VI. Elastic constants of zinc blende III nitrides.

	BN			AlN		GaN	InN
	Present	Experiment[a]	Other calculations	Present	Other calculations[b]	Present	Present
C_{11}^c (GPa)	837	820	830[c], 844[d]	304	348	296	184
C_{12}^c (GPa)	182	190	420[c], 190[d]	152	168	154	116
C_{44}^c (GPa)	493	480	450[c], 483[d]	199	135	206	177
C_{44}^{c0} (GPa)	495			230		225	209
B	400			203		201	139

[a]Grimsditch, Zouboulis, and Polian (Ref. 13).

[b]Hartree-Fock, Ruiz, Alvarez, and Alemany (Ref. 54).

[c]Semiempirical, Sokolovskii (Ref. 69).

[d]Pseudopotential, Rodriguez-Hernández, González-Diaz, and Muñoz (Ref. 42).

with the values given in Table V.

G. Trends

Here, we summarize the trends obtained for the various properties presented above. For most of these, we find that GaN and AlN are very similar to each other, while BN is considerably ''harder'' and InN considerably ''softer.'' The bulk moduli and elastic constants in particular exhibit this trend. Also, the lattice constants and bond lengths of AlN and GaN are close to each other while those of InN are substantially larger (10%) and those for BN substantially smaller (20%) than the first two. The internal strain parameters and the Keating parameters derived from our calculated elastic constants show that BN is strongly resistant to bond-angle distortions while InN is close to the pure bond-stretching limit. The phonon frequencies show a somewhat larger difference between AlN and GaN than other properties and decrease monotonically with increasing cation atomic number.

V. ELECTRONIC PROPERTIES

A. Definition of deformation potentials

The splitting of the bands as a result of a ''pure'' uniaxial strain and the relative shift of the weighted average, e.g., with respect to the valence-band maximum, for hydrostatic strain can be expressed in terms of linear deformation potentials for small strains. In this section we provide the definition of the deformation potentials for specific strains and some eigenstates for zinc-blende crystals using the systematic group-theoretical approach of Kane.[21] Within this framework a hydrostatic strain is described by

$$(\epsilon_1, \epsilon_2, \epsilon_3, \epsilon_4, \epsilon_5, \epsilon_6) = (\eta_1/\sqrt{3}, \eta_1/\sqrt{3}, \eta_1/\sqrt{3}, 0, 0, 0),$$

a volume conserving (tetragonal) strain along the [001] direction by

$$(-\eta_3/\sqrt{6}, -\eta_3/\sqrt{6}, 2\eta_3/\sqrt{6}, 0, 0, 0),$$

TABLE VII. Elastic constants of wurtzite III nitrides. Numbers in parentheses were obtained without internal strain correction and those in square brackets were obtained without relaxation of c/a and u.

	BN	AlN			GaN		InN
	Present	Present	Experiment[a]	Experiment[b]	Present	Experiment[c]	Present
C_{11}^h	987	398	345	411	396	391	271
	(1003)	(427)			(431)		(327)
C_{12}^h	143	140	125	149	144	143	124
	(127)	(111)			(109)		(68)
C_{13}^h	70	127	120	99	100	108	94
	[72]	[70]			[64]		[21]
C_{33}^h	1020	382	395	389	392	399	200
	[1058]	[468]			[476]		[375]
C_{44}^h	369	96	118	125	91	103	46
	(383)	(117)			(116)		(82)
C_{66}^h	422	129	110	131	126	124	74
	(438)	(158)			(161)		(129)
C^h	1445	397			462		209
C^{h0}	1445	458			519		259
B	395	218			207		147

[a]Tsubouchi and Mikoshiba (Ref. 10).

[b]McNeil, Grimsditch, and French (Ref. 11).

[c]Polian, Grimsditch, and Grzegory (Ref. 12).

FIG. 3. Elastic constants of wurtzite III nitrides: comparison between theory and experiment. Open symbols from x-ray analysis by Sheleg and Savastenko (Ref. 8), closed symbols from sound velocity measurements by Polian, Grimsditch, and Grzegory (PGG) (Ref. 12), Grimsditch, Zouboulis, and Polian (GZP) (Ref. 13) (transformed from c-BN), McNeil, Grimsditch, and French (MGF) (Ref. 11), and Tsubouchi and Mikoshiba (TM) (Ref. 10).

and a volume conserving (trigonal) strain along the $[111]$ direction by

$$(0,0,0,\eta_5,\eta_5,\eta_5). \qquad (18)$$

An arbitrary strain tensor can be decomposed into the above irreducible components with magnitudes determined by η_1, η_3, and η_5, where the labels 1, 3, and 5 correspond to Γ_1, Γ_{12}, and Γ_{15}, respectively, in the more commonly used Bouckaert, Smoluchowski, and Wigner notation for the irreducible representations of the tetrahedral group.

The splittings of the most relevant states (highest valence and lowest conduction bands) at Γ, L, and X are summarized in Table IX. For the splittings of the Γ_{15} states, the first column refers to the singlet Γ_1, the second to the doublet Γ_6. For the nondegenerate L_1 state, the first corresponds to
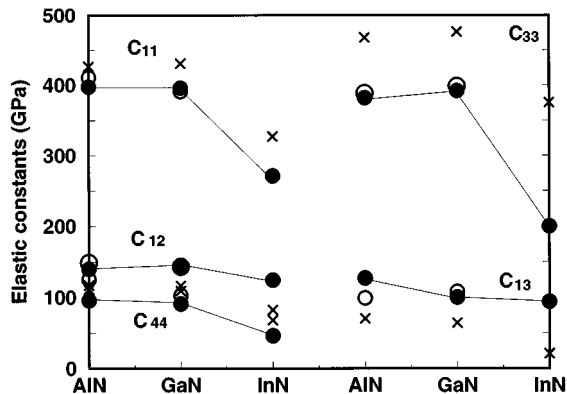
FIG. 4. Elastic constants of the wurtzite III nitrides in various approximations: × denotes C_{ij} transformed from the cubic elastic constants using coordinate rotation, filled circles include Martin's internal strain correction for C_{11}, C_{12}, and C_{44} and direct first-principles values for C_{13} and C_{33}, and open circles are from experiment.
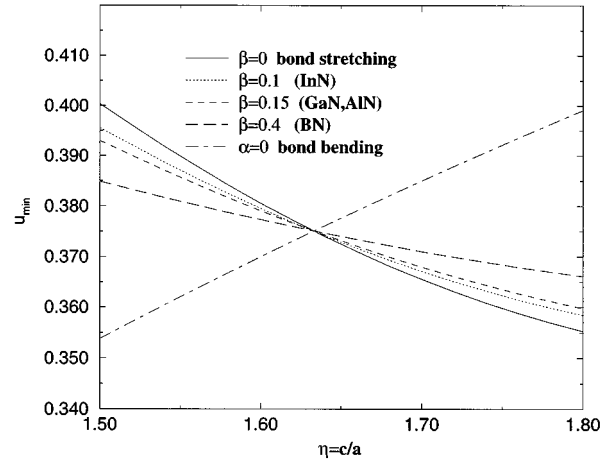
FIG. 5. Keating model predictions for $u_{\min}$ as a function of c/a for various values of β/α.

the k state along the $[111]$ direction parallel to the strain axis while the second to the other $\langle 111 \rangle$ directions whose equivalence to the $[111]$ is lifted by the strain. Similarly for the doubly degenerate L_3 state, the splitting depends on whether we have an L_3 along $[111]$ or along one of the nonequivalent directions, $[\bar{1}11]$, $[1\bar{1}1]$, and $[11\bar{1}]$. For the nondegenerate X_1 state, the first value is for the state along the $[001]$ direction (the strain axis) and the second for the states along the inequivalent $[100]$ and $[010]$ directions. For the doubly degenerate X_5 state under $[001]$ strain, there are again different splittings depending on the location of the X_5 state along the direction of the strain or in orthogonal directions. Under hydrostatic strain, all states are only subject to a shift $d_1\eta_1$ but not to any splittings. Also, Γ_1 is left unaffected by either $[111]$ or $[001]$ strain and L_1 and X_1 are unaffected by $[001]$ and $[111]$ strains, respectively. For the valence-band maximum (Γ_{15}) deformation potentials, the Pikus-Bir[73] notation is more commonly used and it corresponds to the Kane[21] definition as follows:

$$a = d_1/\sqrt{3}, \quad b = d_3/\sqrt{3}, \quad d = d_5/\sqrt{2}, \text{ and } d_o = d_{5o}/\sqrt{2}.$$

Some other relations between definitions of deformation potentials used by different authors are given in Kane,[21] Table XI.

For the splitting of the Γ_{15} state by a trigonal strain, one introduces d_5', the deformation potential corresponding to no internal displacement and d_{5o} corresponding to the optical mode deformation potential. The unprimed d_5 is related to them by

$$d_5 = d_5' - \frac{1}{4}\zeta d_{5o}. \qquad (19)$$

A similar decomposition is used for d_1^5, d_3^5, and d_4.

The calculation of deformation potentials by the present method was tested for silicon. Our results are found to be in good agreement with the available experimental data and will be given elsewhere.

The d_5 deformation potential for the Γ_{15} state is closely related to the wurtzite deformation potential for the uniaxial strain along the c axis. An important difference is that in

TABLE VIII. Keating model parameters: experimental LO- (ω_l) and TO- (ω_t) phonon frequencies from Ref. 5; effective charge parameters S and Z^*; force constant parameters α, β, and β/α, directly calculated (ζ) and its Keating model prediction ζ^K; and Keating model prediction C_{44}^K for C_{44}.

	ω_l (cm^{-1})	ω_t (cm^{-1})	S	Z^*	α (N/m)	β (N/m)	β/α	ζ	ζ^K	C_{44}^K/C_{44}
BN	1304	1056	0.858	2.0	139.6	57.6	0.41	0.1	0.28	0.94
AlN	908	654	1.551	3.2	98.0	15.0	0.15	0.6	0.58	0.79
GaN	731	551	1.246	2.5	96.3	14.8	0.15	0.5	0.63	0.69
InN	694	478	1.983	3.1	79.2	7.1	0.09	0.7	0.70	0.49

wurtzite there is in effect a splitting into a Γ_6 doublet and a Γ_1 singlet in the absence of strain, i.e., for the equilibrium value of c/a and u. Let us define $d_{\Gamma_i}^{6z}=dE_{\Gamma_i}/d\ln\eta|_{V_{eq}}$ as deformation potential for the eigenvalue Γ_i for a distortion along the sixfold axis, $\hat{z}\equiv\hat{c}$, at equilibrium volume. Now consider the traceless strain tensor along [111] in zinc blende given by $(0,0,0,\eta_5,\eta_5,\eta_5)$ as in Eq. (18) transformed to a new z axis along [111], x axis along $[1\bar{1}0]$, and y axis along $[\bar{1}\,\bar{1}2]$. It becomes precisely the strain tensor of Eq. (11) with $\epsilon=2\eta_5$, i.e., $(-\eta_5,-\eta_5,2\eta_5,0,0,0)$. Hence $d\ln\eta=3\eta_5$, and using the results of Table IX for Γ_{15} and [111] strain we expect

$$d_{\Gamma_6}^{6z}=-\frac{1}{\sqrt{6}}d_5 \quad \text{and} \quad d_{\Gamma_1}^{6z}=+\frac{2}{\sqrt{6}}d_5. \tag{20}$$

Since d_5 is negative, this implies that under expansion of c/a, the $E_{\Gamma_6}-E_{\Gamma_1}$ splitting increases.

In analogy with the definition of the d_{5o} optical mode deformation potential, given by

$$\Delta E_{\Gamma_{15}}=\left(\frac{3}{2}\right)^{3/2}\frac{\delta}{4}d_{5o}, \tag{21}$$

TABLE IX. Splittings of energy bands in terms of deformation potentials and irreducible strain components.

Γ_{15}	[001]	$+\sqrt{2}d_3\eta_3$	$-\frac{1}{\sqrt{2}}d_3\eta_3$
	[111]	$+\sqrt{6}d_5\eta_5$	$-\frac{\sqrt{3}}{\sqrt{2}}d_5\eta_5$
L_1	[111]	$+\sqrt{3}d_1^5\eta_5$	$-\frac{1}{\sqrt{3}}d_1^5\eta_5$
L_3	[001]	$+d_3^3\eta_3$	$-d_3^3\eta_3$
	[111]	$+\sqrt{3}d_1^5\eta_5$	$-\frac{1}{\sqrt{3}}d_1^5\eta_5\pm\frac{2\sqrt{2}}{\sqrt{3}}d_3^5\eta_5$
X_1	[001]	$+d_1^3\eta_3$	$-\frac{1}{2}d_1^3\eta_3$
X_5	[001]	$+d_1^3\eta_3$	$-\frac{1}{2}d_1^3\eta_3\pm\frac{\sqrt{3}}{2}d_3\eta_3$
	[111]	$+d_4\eta_5$	$-d_4\eta_5$

where the $\Delta E_{\Gamma_{15}}$ is the splitting of the Γ_{15} state and $\delta=d\ln r$ with r the nearest neighbor bond length, we define the A_1 optical mode deformation potential d^{A_1} by

$$d(E_{\Gamma_6}-E_{\Gamma_1})=d^{A_1}d\ln u. \tag{22}$$

Here, $d\ln u$ is the relative change of the u parameter which equals that of the bond length along the c axis. Hence we expect

$$d^{A_1}=\frac{1}{4}\left(\frac{3}{2}\right)^{3/2}d_{5o}. \tag{23}$$

The spin-orbit coupling produces a further splitting of the Γ_6 state into a Γ_9 and Γ_7 state. The latter then couples to the Γ_7 state derived from the Γ_1. These couplings lead to nonlinear behavior as a function of strain and optical mode distortion which need further study.

B. Results for deformation potentials

The deformation potential results for zinc blende are given in Table X. To identify the state for which deformation potentials are given, its eigenvalue relative to that of the valence-band maximum is also presented. To our knowledge, no experimental data or other calculations for the uniaxial deformation potentials are presently available for these nitrides. We note that only for c-BN is the Γ_{15}^c state the lowest conduction-band state at Γ. In the other compounds, it is the Γ_1 state, which is only subject to hydrostatic strain shifts. The tendency of the p states to lie relatively low in BN is also reflected in the fact that the L_3^c state is located just above the lowest L_1^c state. That the small separation between these states, roughly 0.2 eV, is smaller than splittings of the L_3^c encountered in the computations leads to strong interactions between the states. The resultant nonlinear splittings under [001] and [111] strains are shown in Fig. 6. Since the latter does not reduce the C_{3v} symmetry of the L point along [111], there are no interactions for this point. The interactions occur at the other three L points. The treatment for these two cases, from which the deformation potentials and the interaction parameters can be determined, is discussed in the Appendix.

The calculation of the absolute values of the hydrostatic shifts differs in a significant way from the ones reported

TABLE X. Deformation potentials d for the high-lying valence- and low-lying conduction-band states in the cubic III nitrides for [001] and [111] strains and optical-phonon distortion in eV. The energy E of each state and its relative hydrostatic deformation potential with respect to the valence-band maximum is also given.

State	Strain	E and d (eV)	BN	AlN	GaN	InN
Γ_{15}^v		E	0	0	0	0
	[001]	d_3	-5.9	-2.5	-2.8[a]	-2.3
	[111]	d_5'	-3.3	-4.7	-3.4	-2.7
		d_5	-4.7	-7.5	-5.3	-3.8
	optic	d_{5o}	54.0	19.4	14.6	6.3
Γ_1^c		E	10.9	4.6	2.0	-0.2
		d_1[b]	-8.2	-15.9	-11.1	-5.2
Γ_{15}^c		E	8.8	12.8	10.3	9.5
		d_1[b]	-28.7	-17.4	-11.2	-9.6
	[001]	d_3	4.1	0.5	1.5	1.3
	[111]	d_5'	-21.1	-22.2	-20.7	-19.0
		d_5	-20.1	-22.0	-19.2	-17.6
	optic	d_{5o}	-42.8	-1.3	-11.3	-7.6
L_3^v		E	-2.0	-0.5	-1.0	-0.9
		d_1^{1}[b]	3.3	0.1	2.2	2.5
	[001]	d_3^3	9.6	5.3	4.8	3.4
	[111]	$d_1^{5'}$	13.6	7.0	8.1	6.9
		d_1^5	14.0	8.9	8.1	5.6
		$d_3^{5'}$	1.4	2.2	1.0	0.9
		d_3^5	0.2	4.5	4.4	4.8
	optic	d_{1o}^5	-14.6	-13.3	0.4	6.9
		d_{3o}^5	56.3	-16.7	-27.0	-21.5
L_1^c		E	10.5	7.7	4.8	3.3
		d_1^{1}[b]	-23.0	-15.9	-12.2	-7.7
	[111]	$d_1^{5'}$	16.1	16.4	14.4	8.2
		d_1^5	16.1	14.7	15.9	10.9
	optic	d_{1o}^5	-24.0	12.1	-11.0	-15.0
L_3^{cc}		E	10.7			
X_5^v		E	-5.0	-1.8	-2.8	-2.5
		d_1^{1}[b]	8.7	1.8	6.1	6.4
	[001]	d_1^3	11.3	7.0	6.4	4.8
		d_3	0.2	0.2	0.3	0.5
	[111]	d_4'	19.1	12.8	12.7	10.7
		d_4	19.8	15.1	14.3	11.9
	optic	d_{4o}	-32.0	-16.7	-12.6	-6.8
X_1^c		E	4.4	3.2	3.3	2.9
		d_1^{1}[b]	-2.0	-0.7	-0.5	0.8
	[001]	d_1^3	14.6	4.0	5.6	3.7

[a]An identical value is calculated by Chow, Wright, and Nelson (Ref. 74).

[b]Note that the hydrostatic deformation potentials d_1 and d_1^1 are measured with respect to the valence-band maximum, i.e., the values listed are $d_1 - d_{1,\Gamma_{15}^v}$ and $d_1^1 - d_{1,\Gamma_{15}^v}$, respectively.

[c]The L_3^c is very close to L_1^c only in BN. (See text.)

here, which correspond to traceless (i.e., volume preserving) shear strains. The reason for this was explained in the Introduction. The hydrostatic deformation potentials given in Table X are defined relative to the valence-band maximum.

Of particular interest is the hydrostatic shift of the conduction-band minimum with respect to the valence-band maximum. This is the band-gap deformation potential. Commonly, one gives the value of
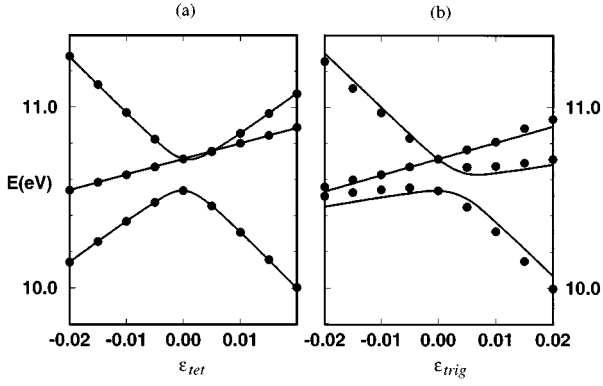
FIG. 6. The behavior of the close-lying L_1^c and L_3^c states in BN (a) under a pure [001] strain and (b) under [111] strain for an L point not along the strain axis. The points are the energies obtained from the first-principles calculation while the solid curves are the analytical energies from Eqs. (A2) and (A3) of the Appendix for $d_1^5 = 16.1$ for L_1^c, $d_3^3 = 10.6$, $d_1^5 = 6.90$, and $d_3^5 = 7.96$ for L_3^c, $|I_{tet}| = 27.0$, and $|I_{trig}| = 13.0$.

$$a_g = dE_g / d \ln\Omega = d_1 / \sqrt{3}, \quad \text{or} \quad dE_g / dp = a_g / B,$$

where B is the bulk modulus. Our values for these parameters are compared with those in the literature in Table XI.

As mentioned in the Introduction, the calculation of the absolute hydrostatic deformation potentials requires an interface calculation between compressed and expanded regions of the crystal, in order to determine their band lineup. As a result they are generally orientation dependent. However, within a simple treatment of the band-offset problem, based on the idea of aligning a suitable internal reference level in each part of the solid, one can obtain a first approximation of these important deformation potentials. In the charge neutrality point (CNP) model of Flores and Tejedor,[75] one assumes that a certain energy level in the middle of the gap (called the CNP) should be aligned across the interface. The idea behind this is that the states above this level will lead to an accumulation of negative charge when they are filled while the states below it when empty will tend to produce a positive

charge.[76] In a variant of this model, called the dielectric midpoint energy model,[22] this CNP is identified with the average of the highest valence and lowest conduction band over the Brillouin zone. By calculating this level and the valence-band maximum at two different lattice constants and assuming the DME's to align, we obtain the absolute hydrostatic deformation potential $a_v = dE_v / d \ln\Omega$ for the valence-band maximum. We have carried out this calculation for the zinc-blende form, using the Baldereschi-point Brillouin zone average[77] to define the dielectric midgap point. The resulting values for a_v are 0.9 eV for BN, 1.6 eV for AlN, 0.8 eV for GaN, and 0.5 eV for InN. We note that the uncertainty in this DME calculation on the deformation potential is at least 2 eV, which for the present values implies that the sign can be reversed. From previous experience, we expect that the DME gives an underestimate.[78] At this point, we can thus only conclude that the a_v for the nitrides are of the order of 1 eV, which is small compared to some of the relative deformation potentials, given in Table X. For wurtzite, one may assume that the above applies to the weighted average of the Γ_6 and Γ_1 crystal field split states. By taking into account the relative hydrostatic deformation potential d_1, one can obtain an estimate of the absolute hydrostatic deformation potential of any state of interest, e.g., the conduction-band minimum. For example, one would obtain that $a_c = dE_c / d \ln\Omega \approx -9$ eV, -6 eV, and -3 eV for the conduction-band minimum at Γ for AlN, GaN, and InN, respectively. These values should apply equally to wurtzite as well as to zinc blende to first approximation.

VI. CONCLUSIONS

In this paper we have presented a theoretical study of the elastic constants and the related vibrational and electronic properties for the group III nitrides (BN, AlN, GaN, and InN) using the full-potential LMTO method. Fully relaxed lattice constants and bulk moduli were obtained for both the zinc-blende and wurtzite structures and shown to be in good agreement with other calculations and experimental data where they were available. A relation of the TO A_1 phonon

TABLE XI. Band-gap deformation potential and pressure coefficients.

			BN[a]	AlN[b]	GaN	InN
a_g (eV)	zinc blende	present	−1.2	−0.38	−6.4	−3.0
		other[c]	−1.1	−0.37	−7.4	−2.2
	wurtzite	present	1.5	−9.0	−6.9	−2.8
		other[d]	1.4	−7.1 to −9.5	−7.8,−9.8	−4.1,−4.25
dE_g / dp (meV/GPa)	zinc blende	present	3.0	1.9	32	22
		other[c]	2.8	1.7	40	16
	wurtzite	present	3.8	44	33	19
		other[d]	3.7	36 to 43	39 to 47	25,33

[a]For X_1 conduction-band minimum in zinc blende and for K_1 conduction-band minimim in wurtzite structures.
[b]For X_1 conduction-band minimum in zinc blende.
[c]Theory from Ref. 43.
[d]Experiment and theory from Ref. 5, Chap. 4 and Ref. 43.

to the c/a relaxation in wurtzite and the elastic constant associated with the uniaxial strain along the c axis was derived. The calculated TO phonons in wurtzite and zinc blende were found to be in agreement with experimental data and other recent calculations within a few percent. The mode Grüneisen parameters of these phonons were also obtained. The elastic constants of the zinc-blende structure were obtained directly from first-principles calculations of the total energy under appropriate strain distortions and were found to be in good agreement with experiment for c-BN. The elastic constants C_{11}^h, C_{12}^h, and C_{44}^h of wurtzite obtained from those of zinc blende merely by the transformation to the coordinates adapted to the hexagonal symmetry were found to be quite close to the experimental values. A small improvement resulted from Martin's internal strain correction.[20] Explicit calculations for the wurtzite crystals under hexagonal symmetry-preserving distortions show that C_{13}^h and C_{33}^h are significantly affected by the nonideal c/a ratios. Very good agreement was shown for AlN and GaN with recent experimental data obtained from sound velocity measurements. The older literature values derived from x-ray diffraction data, however, were found to be rather inaccurate. Our calculations for InN, the zinc-blende forms of AlN and GaN, and wurtzite BN contain predictions yet to be verified by experiment.

The force constant parameters of the well-known Keating model were derived from our calculated elastic constants and experimental LO-phonon–TO-phonon splittings. We found that the Keating model does not describe the shear elastic constant C_{44}^c very well for these materials and becomes poorer as we proceed from BN to InN. The Keating model shows that the ratio of bond-bending to bond-stretching forces β/α is significantly larger in BN than in AlN and GaN which in turn are larger than that in InN. This behavior also explains the trend in the values of the internal strain parameters: the Kleinman ζ parameter for zinc blende and a similar parameter $\xi = -du_{\min}/d(c/a)$ for wurtzite introduced in the present work.

The strain and optical-phonon induced changes in the band structure were determined for small strains and expressed in terms of uniaxial deformation potentials for the Γ, L, and X eigenvalues of zinc-blende crystals near the band gap. These provide values for these parameters which to date have neither been measured nor calculated. The band-gap hydrostatic deformation potentials and pressure coefficients were also obtained and compared to experimental data and previous calculations. The deformation potentials of the valence-band maximum for [111] strain and for the transverse-optical mode can be used to obtain estimates of those in wurtzite structure, respectively, for c/a distortion and for the A_1 tranverse optical mode. A rough estimate is provided for the absolute hydrostatic deformation potentials

of the valence-band maximum using the dielectric midgap approach.

APPENDIX

In this appendix we discuss the behavior of nearly degenerate L_1 and L_3 levels, as occurs in the conduction band of c-BN, under strain. In the presence of a [001] strain the symmetry of the point L is reduced to the group containing only the identity and a reflection plane. The same is true under a [111] strain for the L points not on the [111] axis. For the L on that axis the symmetry is unaffected. Thus the L_3^c state even under the reflection interacts with the L_1^c state. The odd state does not and hence undergoes a linear shift. The interaction between the two even states for both situations is given by the simple secular equation

$$\begin{vmatrix} -d(L_1)\epsilon - E & I\epsilon \\ I^*\epsilon & \Delta - d(L_{3e})\epsilon - E \end{vmatrix} = 0, \quad (A1)$$

where Δ is the $L_3 - L_1$ separation at $\epsilon = 0$ and $I\epsilon$ is the coupling strength. The energies for the two states relative to $E(L_1^c)$ at zero strain are

$$E_{1,2} = \frac{1}{2}\{[\Delta - d(L_1)\epsilon - d(L_{3e})\epsilon]$$
$$\pm \sqrt{[\Delta - d(L_1)\epsilon - d(L_{3e})\epsilon]^2 + 4|I|^2\epsilon^2}\}, \quad (A2)$$

while that for the odd state is

$$E_3 = \Delta + d(L_{3o})\epsilon. \quad (A3)$$

For the tetragonal strain, $d(L_1) = 0$ and $d(L_{3e}) = d(L_{3o}) = d_3^3$ with $\epsilon = \eta_3$. For the trigonal strain, $d(L_1) = (1/\sqrt{3})d_1^5$, $d(L_{3e}) = (1/\sqrt{3})d_1^5 + (2\sqrt{2}/\sqrt{3})d_3^5$, and $d(L_{3o}) = -(1/\sqrt{3})d_1^5 + (2\sqrt{2}/\sqrt{3})d_3^5$ with $\epsilon = \eta_5$. In accordance with Eq. (A3), one of the L_3^c levels is found to vary linearly with strain, allowing a simple determination of the deformation potential $d(L_{3o})$. A fit of the behavior of the other two levels as a function of ϵ with $|I| = 13.0$ for trigonal and $|I| = 27.0$ for tetragonal strains is shown in Fig. 6.

---

[1] *Diamond, Silicon Carbide and Nitride Wide-Bandgap Semiconductors,* edited by C. H. Carter, Jr., G. Gildenblat, S. Nakamura, and R. J. Nemanich, MRS Symposium Proceedings No. 339 (Materials Research Society, Pittsburgh, 1994).

[2] *Wide-band-gap Semiconductors*, Proceedings of the Seventh Tri-

este Semiconductor Symposium (1992), edited by C. G. Van de Walle (North-Holland, Amsterdam, 1993); also published as Physica B **185**, 1 (1993).

[3] *Wide Band Gap Semiconductors*, edited by T. D. Moustakas, J. H. Pankove, and Y. Hamakawa, MRS Symposium Proceedings No.

242 (Materials Research Society, Pittsburgh, 1992).

[4] *Wide Band Gap Electronic Materials*, Vol. 1 of *NATO Advanced Study Institute, Series 3: High Technology,* edited by M. A. Prelas, P. Gielisse, G. Ppovici, B. V. Spitsyn, and T. Stacy (Kluwer Academic Publishers, Dordrecht, 1995).

[5] *Properties of Group III Nitrides,* edited by J. H. Edgar, Electronic Materials Information Service (EMIS) Datareviews Series (Institution of Electrical Engineers, London, 1994).

[6] W. A. Brantley, J. Appl. Phys. **44**, 534 (1973).

[7] W. R. L. Lambrecht and B. Segall, in *Properties of Group III Nitrides,* Ref. 5, Chap. 4, pp. 125–158.

[8] V. A. Savastenko and A. U. Sheleg, Phys. Status Solidi A **48**, K135 (1978); A. U. Sheleg and V. A. Savastenko, Izv. Akad. Nauk SSSR Neorg. Mater. **15**, 1598 (1979) [Inorg. Mater. (USSR) **15**, 1257 (1979)].

[9] M. E. Sherwin and T. J. Drummond, J. Appl. Phys. **69**, 8423 (1991).

[10] K. Tsubouchi and N. Mikoshiba, IEEE Trans. Sonics Ultrason. **SU-32**, 634 (1985).

[11] L. E. McNeil, M. Grimsditch, and R. H. French, J. Am. Ceram. Soc. **76**, 1132 (1993).

[12] A. Polian, M. Grimsditch, and I. Grzegory, J. Appl. Phys. (to be published).

[13] M. Grimsditch, E. S. Zouboulis, and A. Polian, J. Appl. Phys. **76**, 832 (1994).

[14] P. Perlin, I. Gorczyca, N. E. Christensen, I. Grzegory, H. Teisseyre, and T. Suski, Phys. Rev. B **45**, 13 307 (1992).

[15] K. Kim, W. R. L. Lambrecht, and B. Segall, Phys. Rev. B **50**, 1502 (1994).

[16] P. Hohenberg and W. Kohn, Phys. Rev. **136**, B864 (1964); W. Kohn and L. J. Sham, *ibid.* **140**, A1133 (1965).

[17] O. K. Andersen, O. Jepsen, and M. Šob, in *Electronic Band Structure and its Applications*, edited by M. Yussouff (Springer, Heidelberg, 1987), p. 1.

[18] M. Methfessel, Phys. Rev. B **38**, 1537 (1988).

[19] L. Kleinman, Phys. Rev. **128**, 2614 (1962).

[20] R. M. Martin, Phys. Rev. B **6**, 4546 (1972).

[21] E. O. Kane, Phys. Rev. **178**, 1368 (1969).

[22] M. Cardona and N. E. Christensen, Phys. Rev. B **35**, 6182 (1987).

[23] L. Hedin and B. I. Lundqvist, J. Phys. C **4**, 2064 (1971).

[24] W. R. L. Lambrecht and B. Segall, in *Wide Band Gap Semiconductors*, Ref. 3, p. 367.

[25] W. R. L. Lambrecht, B. Segall, S. Strite, G. Martin, A. Agarwal, H. Morkoç, and A. Rockett, Phys. Rev. B **50**, 14 155 (1994).

[26] V. Fiorentini, M. Methfessel, and M. Scheffler, Phys. Rev. B **47**, 13 353 (1993).

[27] D. J. Chadi and M. L. Cohen, Phys. Rev. B **7**, 692 (1973).

[28] J. Harris, Phys. Rev. B **31**, 1770 (1985).

[29] M. Methfessel and M. van Schilfgaarde, Phys. Rev. B **48**, 4937 (1993).

[30] J. F. Nye, *Physical Properties of Crystals* (Clarendon, Oxford, 1957), Chap. VIII.

[31] T. Lei, T. D. Moustakas, R. J. Graham, Y. He, and S. J. Berkowitz, J. Appl. Phys. **71**, 4933 (1992).

[32] S. Strite, J. Ruan, D. J. Smith, J. Sariel, N. Manning, H. Chen, W. J. Choyke, and H. Morkoç, Bull. Am. Phys. Soc. **37**, 346 (1992).

[33] B. N. Onwuagba, Solid State Commun. **89**, 289 (1994).

[34] W. R. L. Lambrecht and B. Segall, Phys. Rev. B **40**, 9909 (1989); and in *Wide Band Gap Electronic Materials*, Ref. 4, p. 335.

[35] K. T. Park, K. Terakura, and N. Hamada, J. Phys. C **20**, 1241 (1987).

[36] R. M. Wentzcovitch, M. L. Cohen, and P. K. Lam, Phys. Rev. B **36**, 6058 (1987).

[37] P. K. Lam, R. M. Wentzcovitch, and M. L. Cohen, in *Materials Science Forum*, edited by J. J. Pouch and S. A. Alterovitz (Trans Tech, Zurich, 1990), Vols. 54&55. p. 165.

[38] E. Knittle, R. M. Wentzcovitch, R. Jeanloz, and M. L. Cohen, Nature (London) **337**, 349 (1989).

[39] P. E. van Camp, V. E. Van Doren, and J. T. Devreese, Solid State Commun. **71**, 1055 (1989).

[40] K. Kikuchi, T. Uda, A. Sakuma, M. Hirao, and Y. Murayama, Solid State Commun. **81**, 653 (1992).

[41] S. Matar, V. Fonnet, and G. Demazeau, J. Phys. I (France) **4**, 335 (1994).

[42] P. Rodriguez-Hernández, M. González-Diaz, and A. Muñoz, Phys. Rev. B **51**, 14705 (1995).

[43] N. E. Christensen and I. Gorczyca, Phys. Rev. B **50**, 4397 (1994).

[44] W. R. L. Lambrecht and B. Segall, Phys. Rev. B **43**, 7070 (1991).

[45] N. E. Christensen and I. Gorczyca, Phys. Rev. B **47**, 4307 (1993).

[46] C.-Y. Yeh, Z. W. Lu, S. Froyen, and A. Zunger, Phys. Rev. B **46**, 10 086 (1992).

[47] A. F. Wright and J. S. Nelson, Phys. Rev. B **50**, 2159 (1994); **51**, 7866 (1995).

[48] K. Miwa and A. Fukumoto, Phys. Rev. B **48**, 7897 (1993).

[49] A. Muñoz and K. Kunc, Phys. Rev. B **44**, 10 372 (1991).

[50] P. E. Van Camp, V. E. van Doren, and J. T. Devreese, Solid State Commun. **81**, 23 (1992).

[51] B. J. Min, C. T. Chan, and K. M. Ho, Phys. Rev. B **45**, 1159 (1992).

[52] M. Palummo, C. M. Bertoni, L. Reining, and F. Finocchi, in *Wide-band-gap Semiconductors*, Ref. 2, p. 404.

[53] A. Muñoz and K. Kunc, J. Phys. Condens. Matter **5**, 6015 (1993).

[54] E. Ruiz, S. Alvarez, and P. Alemany, Phys. Rev. B **49**, 7115 (1994).

[55] I. V. Aleksandrov, A. F. Goncharov, S. M. Stishov, and E. V. Yakovenko, Pis'ma Zh. Éksp. Teor. Fiz. **50**, 116 (1989) [JETP Lett. **50**, 127 (1989)]; E. V. Yakovenko, I. V. Aleksandrov, A. F. Goncharov, and S. M. Stishov, Zh. Éksp. Teor. Fiz. **95**, 2097 (1989) [Sov. Phys. JETP **68**, 1213 (1989)].

[56] A. D. Alvarenga, M. Grimsditch, and A. Polian, J. Appl. Phys. **72**, 1955 (1992).

[57] Masaki Ueno, Minoru Yoshida, Akifumi Onodera, Osamu Shimomura, and Kenichi Takemura, Phys. Rev. B **49**, 14 (1994).

[58] G. A. Slack (private communication).

[59] Q. Xia, H. Xia, and A. L. Ruoff, J. Appl. Phys. **73**, 8198 (1993).

[60] H. Xia, Q. Xia, and A. L. Ruoff, Phys. Rev. B **47**, 12 925 (1993).

[61] P. Perlin, C. Jauberthie-Carillon, J. P. Itie, A. San Miguel, I. Grzegory, and A. Polian, Phys. Rev. B **45**, 83 (1992).

[62] J. H. Rose, J. R. Smith, F. Guinea, and J. Ferrante, Phys. Rev. B **29**, 2963 (1984).

[63] I. Gorczyca, N. E. Christensen, E. L. Peltzer y Blanca, and C. O. Rodriguez, Phys. Rev. B **51**, 11 936 (1995).

[64] J. A. Sanjurjo, E. López-Cruz, P. Vogl, and M. Cardona, Phys. Rev. B **28**, 4579 (1983).

[65] S. Murugkar, R. Merlin, T. Lei, and T. D. Moustakas, Bull. Am. Phys. Soc. **37**, 556 (1992).

[66] P. Perlin, A. Polian, and T. Suski, Phys. Rev. B **47**, 2874 (1993).

[67] K. Hayashi, K. Itoh, S. Sawaki, and I. Akasaki, Solid State Commun. **77**, 115 (1991).

[68] T. Inushima, A. Nagase, A. Iso, T. Yaguchi, and T. Shiraishi, in *Proceedings of the 6th International Conference on Silicon Car-*

bide and Related Materials, Kyoto 1995 (Institute of Physics, London, in press).

[69] T. D. Sokolovskii, Izv. Akad. Nauk SSSR Neorg. Mater. **19**, 1484 (1983) [Inorg. Mater. (USSR) **19**, 1311 (1983)].

[70] Atomic displacements from equilibrium positions were inferred from the data. With these, combined with data on bulk moduli and expansion coefficients and certain confining relations, a full set of six C_{ij}'s were extracted. It would appear that such results would be subject to considerable uncertainties. Discrepancies in the results for other materials were found. For example, the C_{12} and C_{44} for Zn obtained by that approach were 60% lower than the values obtained by velocity of sound measurements.

[71] P. N. Keating, Phys. Rev. **145**, 637 (1966).

[72] R. M. Martin, Phys. Rev. B **1**, 4005 (1970).

[73] G. E. Pikus and G. L. Bir, Fiz. Tverd. Tela (Leningrad) **1**, 1642 (1959) [Sov. Phys. Solid State **1**, 1502 (1959)].

[74] W. W. Chow, A. F. Wright, and J. S. Nelson, Appl. Phys. Lett. **68**, 296 (1996).

[75] F. Flores and C. Tejedor, J. Phys. C **20**, 145 (1987).

[76] J. Tersoff, Phys. Rev. Lett. **30**, 4874 (1984).

[77] A. Baldereschi, Phys. Rev. B **7**, 5212 (1973).

[78] W. R. L. Lambrecht, B. Segall, M. Methfessel, and M. van Schilfgaarde, Phys. Rev. B **44**, 3685 (1991).